Chapter 7

Computational binding study of Anvylic-3288 with α7-nicotinic acetylcholine receptor

7. Computational binding study of Anvylic-3288 with α7-nicotinic acetylcholine receptor

7.1. Introduction

The α7 Nicotinic Acetylcholine Receptor (nAChR), a class of nicotinic receptors, is involved in cognition. The receptor is implicated in many diseases, including AD, Parkinsonism, Schizophrenia, Autism, Rett syndrome etc. The α7-nAChR is a homo-pentameric receptor of about ~55 – 60 KDa and is made up of five α7 subunits [243, 244]. Each α7 subunit is made up of four trans-membranous domains with a large cytoplasmic loop between M3 and M4 domains [245]. The orthostatic ligand binding site is present at the interface of principal and complementary subunits in the extracellular region. These are fast desensitising receptors on prolonged activation by agonist and also show higher permeability of Ca^{2+} ions [244]. In AD, the Aβ interacts with α7-nAChR and alters its function in the brain [196, 246]. The condition further deteriorates due to the low level of ACh, hampering the normal neuronal conduction mediated by these receptors [247-249]. Interaction of Aβ with α7-nAChR also mediates tau phosphorylation through a tau protein kinase and treatment with α7-nAChR antagonist decreases the aforementioned phenomenon [250].

The orthostatic binding site agonists of α7-nAChR exert similar action to those of endogenous agonists but lead to fast desensitisation of the receptor due to prolonged binding and are not beneficial (**Figure 7.1**). Further, their actions are not synchronised with the normal physiological processes and produce unwanted effects [27]. Allosteric modulation is based on the fact that the protein exists in multiple conformations and the binding of a ligand stabilises a particular conformation, i.e., an active or closed state. The site is other than the binding site of conventional ligands referred to as the allosteric site. Positive allosteric modulators (PAMs) bind to an allosteric site in order to keep the receptor in an open state and show the effect only upon binding of an endogenous ligand

to the receptor [28]. PAMs are of two types in case of α7-nAChR. Type I PAM increases the response, i.e., peak current of the endogenous ligand through receptor conformation changes from inactive to active state but does not alter the response time. Type II PAM increases the response, i.e., peak current as well as the duration of response by delaying receptor desensitisation. Type II PAM prolongs the opening of α7-nAChR, which also allows passage of Ca^{2+} ions and may lead to cell toxicity [29].

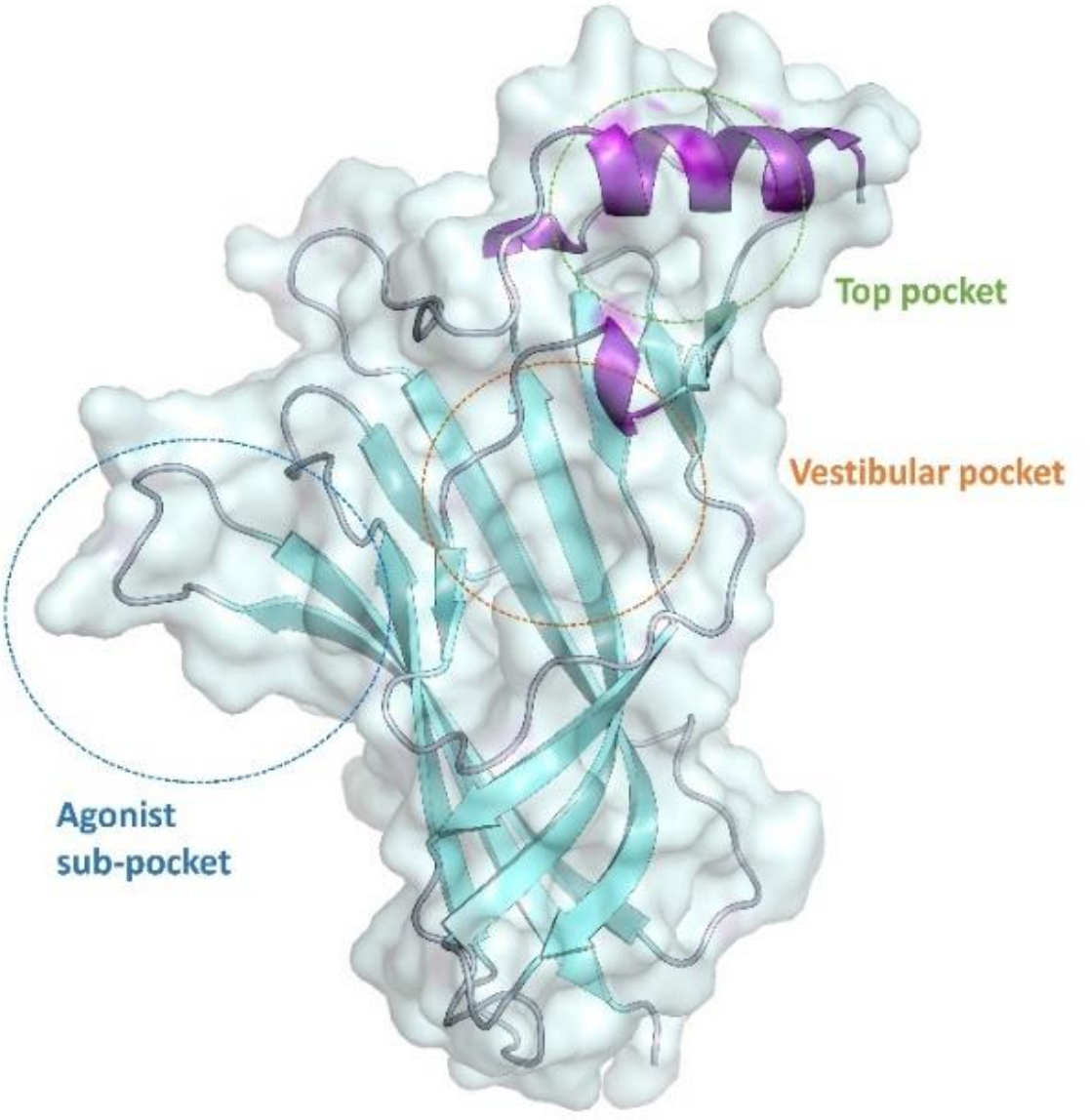

Figure 7.1 Structural representation of α7-subunit of α7-nAChR showing top, vestibular, and agonist sub-pocket binding sites.

AVL-3288 is an allosteric modulator of α7-nAChR, which potentiates the peak current generated by binding with ACh. The molecule has shown encouraging results in pre-

clinical studies [30]. The first human clinical trial of AVL-3288 has shown that it could be safely administered to humans and possesses 'potential positive neurocognitive effects' in CNS disorders [31]. The molecule is undergoing clinical trial in schizophrenia patients which is a 'single-centre, outpatient, randomised, double-blind, placebo-controlled, 3-treatment-phase, cross-over study' (clinical study identifier: NCT02978599). The binding profile of AVL-3288 with α7-nAChR through *in silico* approaches was investigated.

7.2. Material and methods

7.2.1. Protein preparation

The protein-ligand complex for α7-nAChR (PDB id – 5AFK) was obtained from Protein Databank (https://www.rcsb.org/). It was pre-processed by using the protein preparation wizard utility of Schrodinger's maestro (academic version). The obtained protein structure was converted to pdbqt format by merging non-polar hydrogen in AutoDockTools-1.5.6 [196].

7.2.2. Ligand preparation

The selected compound AVL-3288 was sketched in ChemDraw 18.0 and imported in Chem3D 18.0. The energy minimisation was performed using the MM2 module and was converted to a mol2 file.

7.2.3. Molecular docking

The grids were generated for atom types, i.e. A, C, HD, NA, N, Cl and OA using AutoGrid 4.0. Further, the grids were calculated for three different sites viz. top, vestibule, and agonist sub-pocket of the receptor (**Table T29 in appendix**) [188]. The molecular docking was performed by using AutoDock suite 4.2.6, employing Lamarckian Genetic Algorithm (LGA) for conformational search. LGA parameters used for dockings are summarised in the table (**Table T30 in appendix).** The post-docking analysis and

visualisation were performed by Autodock tools 1.5.6 and Discovery Studio visualiser [235].

7.2.4. Alanine scanning

Alanine scanning was carried out for residues interacting with the ligands, and individual residues were mutated to alanine. The mutated complexes were used to build the topology and coordinates files by *tleap*. The MMGBSA.py, a python script, was used to perform virtual alanine scanning for eighteen frames at an equal time interval and a salt concentration of 0.15 mM for MM/PBSA calculations.

7.2.5. Molecular dynamics

MD simulations were carried out to evaluate chemistry at the molecular level. MD was performed for complexes through Amber18. The protein-ligand complexes were soaked in TIP3P hydrated cubic box with a cut-off distance of 12 Å. The residual charges of the system were neutralised by using counter ions placed in the system. The particle mesh Ewald (PME) was used to handle long-range electrostatic interactions. The MD systems were subjected to energy minimisation followed by heating, density equilibration, and equilibration under periodic boundary conditions. The detailed experimental protocols are summarised in tables (**Table T31 and T32 in appendix**). Further, the final production phase of 50 ns was carried out at 310.15 K as an NPT ensemble [238, 251].

7.2.6. MM-PBSA

The MD simulations obtained were subjected to free energy calculations. Eighteen frames, at an equal time interval, were considered for calculations with a salt concentration of 0.15 mM. The Poisson-Boltzmann (PB) model was used for MM/PBSA calculations. The entropy calculation was neglected in both cases [238, 251].

7.3. Results and discussion

The docking studies on the three sites, i.e., top, vestibule and agonist sub-pocket, displayed higher affinity towards sub-pocket near agonist binding site for a1 pose (**Table 7.1**).

Table 7.1 Mean binding energies, cluster size, lowest binding energy and free binding energies of ligands against α7-nAChR (PDB id - 5AFH).

Pose	Mean binding energy (Kcal/mol)	Cluster count	Lowest binding energy (Kcal/mol)	$\Delta G_{MM/PBSA}$ (Kcal/mol)
t1	-6.28 ± 0.37	186	-6.9	-20.04 ± 6.09
v1	-8.17 ± 0.37	170	-8.63	-13.99 ± 4.82
a1	-8.36 ± 0.16	242	-8.85	-22.04 ± 4.07

7.3.1. Binding mode in the top pocket

The t1 binding mode of AVL-3288 with α7-nAChR displayed hydrogen bonding with A:Tyr62 residue in the top pocket. It also displayed carbon-hydrogen bond with A:Lys12 residue. The other essential interactions were π-π stacking with A:Tyr62, π-alkyl contacts with A:Leu10, A:Tyr70, π-cation interaction with B:Arg4, and alkyl mediated non-bonding interaction with A:Leu6. This was the most prominent pose for the top pocket with a cluster count of 178. The other poses t2, t3 and t4 have cluster counts of 70, 58, 49 out of 500 generated poses during docking (**Figure 7.2**). In case of the t2 pose, A:Glu9 and A:Asn13 formed a hydrogen bond with secondary amine and oxazole nitrogen atom. It also displayed π-π stacking with A:Tyr62. The other interactions include π-alkyl with A:His61, A:Tyr62, A:Trp65 and A:Tyr70 and alkyl interactions with A:Leu6 and A:Lys12. In case of t3 pose, similar but fewer interactions were observed including hydrogen bond interactions with A:His61, A:Tyr62 and A:Gln64, π-π stacking with A:His61, π-alkyl with A:His61, A:Tyr70, alky interaction with A:leu6 and π-lone pair interaction with A:Gln64. Further, pose t4 displayed quite a different interaction pattern. It displayed hydrogen bonding with A:Glu9 and A:Lys12. The other interacting residues

were A:His61, A:Tyr62 (π-π and π-alkyl), A:Leu6, A:Leu10, A:Lys:12 (alkyl), A:Leu10 (π-σ, carbon-H bond) and A:Glu9 (π-lone pair).

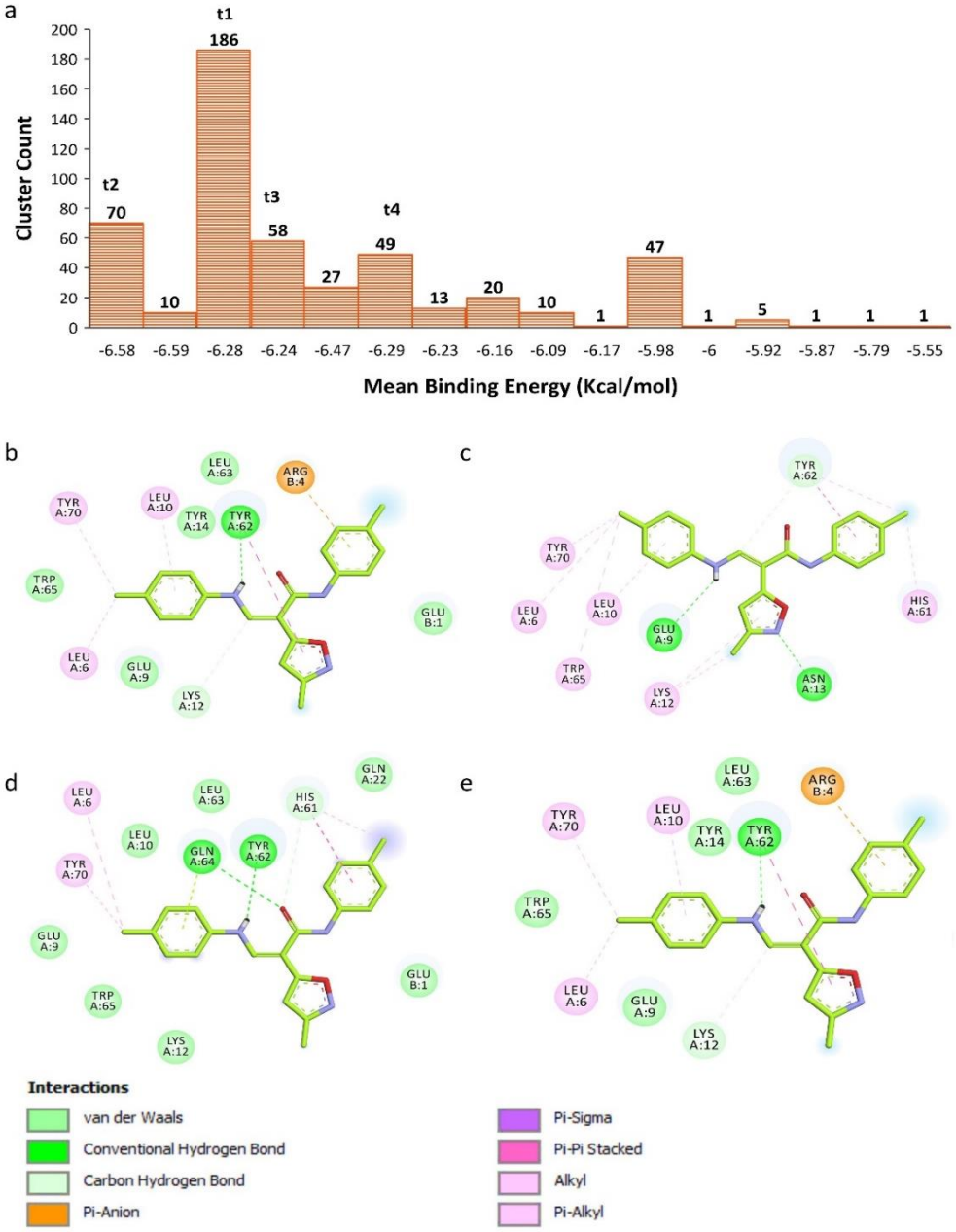

Figure 7.2 (a) Cluster distribution vs. mean binding energy of various poses of AVL-3288 in the top pocket of α7-nAChR (PDB id – 5AFK), (b, c, d, & e) 2-D interaction diagram of t1, t2, t3, and t4 poses in the top pocket.

7.3.2. Binding mode in vestibule pocket

The binding mode v1 of AVL-3288, when bound to vestibule pocket, showed hydrogen bond interactions with A:Pro86, A:Leu88 and A:Ala90. The other essential interactions include π-alkyl with A:Trp84, A:Val85, A:Leu88, A:Pro97, A:Tyr115, B:Pro102, and

B:Leu104 and alkyl interactions with A:Met56, A:Ala90, A:Ala93, A:Pro97 and B:Leu104. The atypical interactions are observed with A:Met56 through π-sulphur interaction, π-lone pair interaction with A:Pro86, and π-σ interaction with A:Ala89. The other important binding poses were v2, v3 and v4 with cluster counts of 88, 65, and 50, respectively. The pose v2 displayed conventional hydrogen bonds with A:Val85, A:Pro86, and B:Gln103, while carbon-hydrogen bond with A:Pro86. The residues A:Trp84, A:His147, B:Pro102 displayed π-alkyl and A:Leu54, A:Ile119, B:pro79, B:Leu104 showed alkyl interactions. The π-σ and π-lone pair interactions with B:Leu104, A:Leu88, respectively, were also observed instead of A:Ala89 and A:Pro86 as in case of pose v1. But, the interaction with A:Met56 was retained. The third pose, i.e., v3 displayed alkyl interactions with A:Leu54, A:Val85, A:Lys96, A:Pro97 and A:Ile119 and π-σ interactions with A:Phe52, A:Phe142, A:Ala90, A:Pro97, B:Pro102, B:Leu104. The v4 pose of AVL-3288 displayed two hydrogen bonds with B:Gln103 and A:Pro86, π-σ interactions with B:Leu104, B:Pro102, A:Pro97, B:Pro102 and alkyl interactions with A:Ala90, B:Leu104 and A:Pro97 (**Figure 7.3**).

7.3.3. Binding mode in agonist sub-pocket

The binding mode a1 of AVL-3288, when bound to agonist sub-pocket, showed the presence of π-donor hydrogen bonds with A:Tyr184 along with π-π stacking between A:Tyr91, A:Trp145 with one of the phenyl ring of the ligand. A:Tyr184, B:Leu36, B:Leu116 displayed alkyl interactions and A:Trp145 showed π-σ interaction. The a2 binding pose displayed quite different interactions compared to a1 pose with A:Tyr91 and B:Trp53 showed π-lone pair and π-cation interaction, respectively. It also displayed π-π stacking with A:Tyr184, B:Trp53; π-alkyl interactions with A:Tyr184, A:Tyr191, B:Leu36; and alkyl interactions with A:Ala93, B:Leu100. Further, the a3 binding pose of AVL-3288 did not display any hydrogen bond interactions but π-π stacking, π-alkyl and π-σ interactions were prominent (**Figure 7.4**).

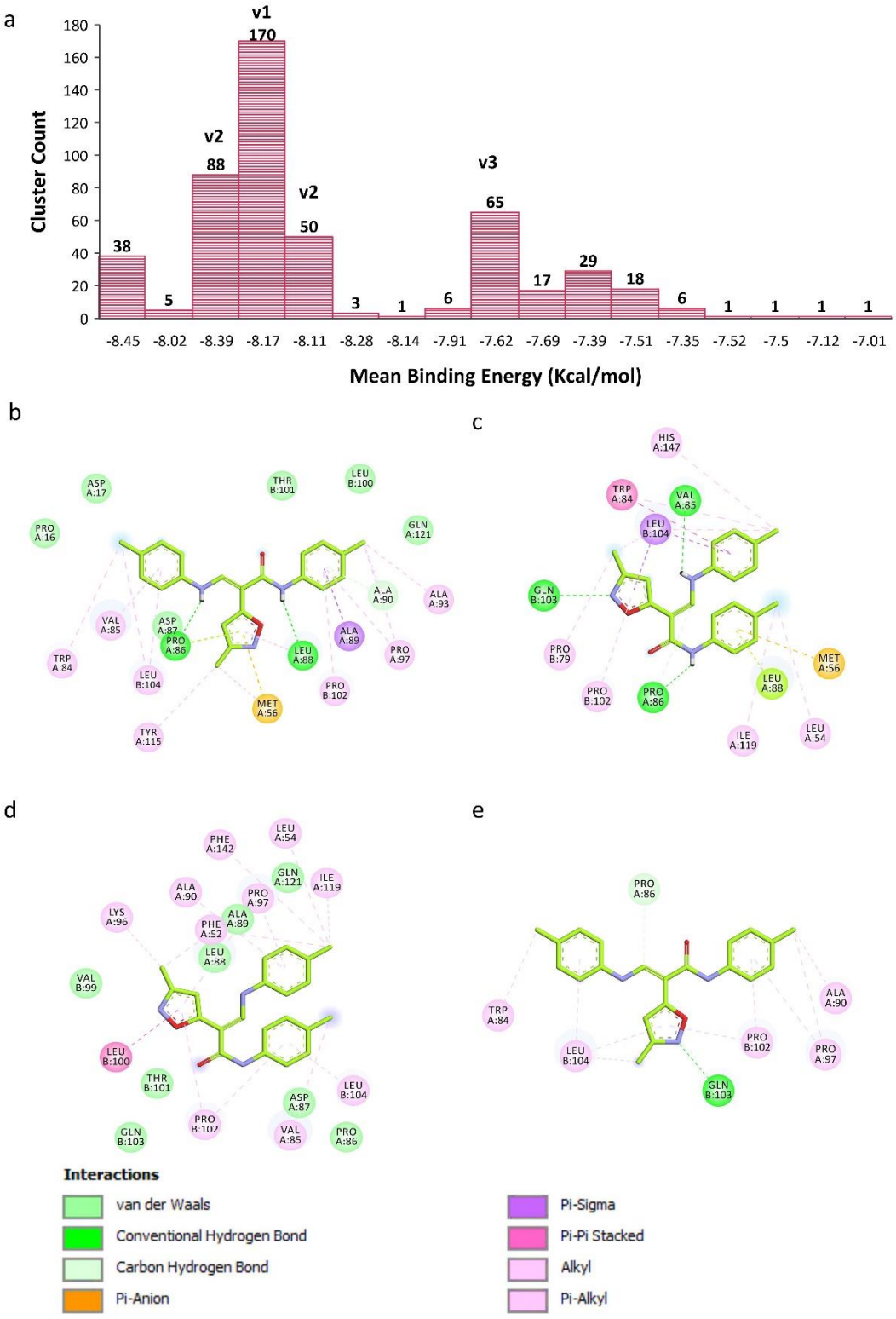

Figure 7.3 (a) Cluster distribution vs. mean binding energy of various poses of AVL-3288 in vestibule pocket of α7-nAChR (PDB id – 5AFK), (b, c, d, & e) 2-D interaction diagram of v1, v2, v3, and v4 poses in vestibule pocket.

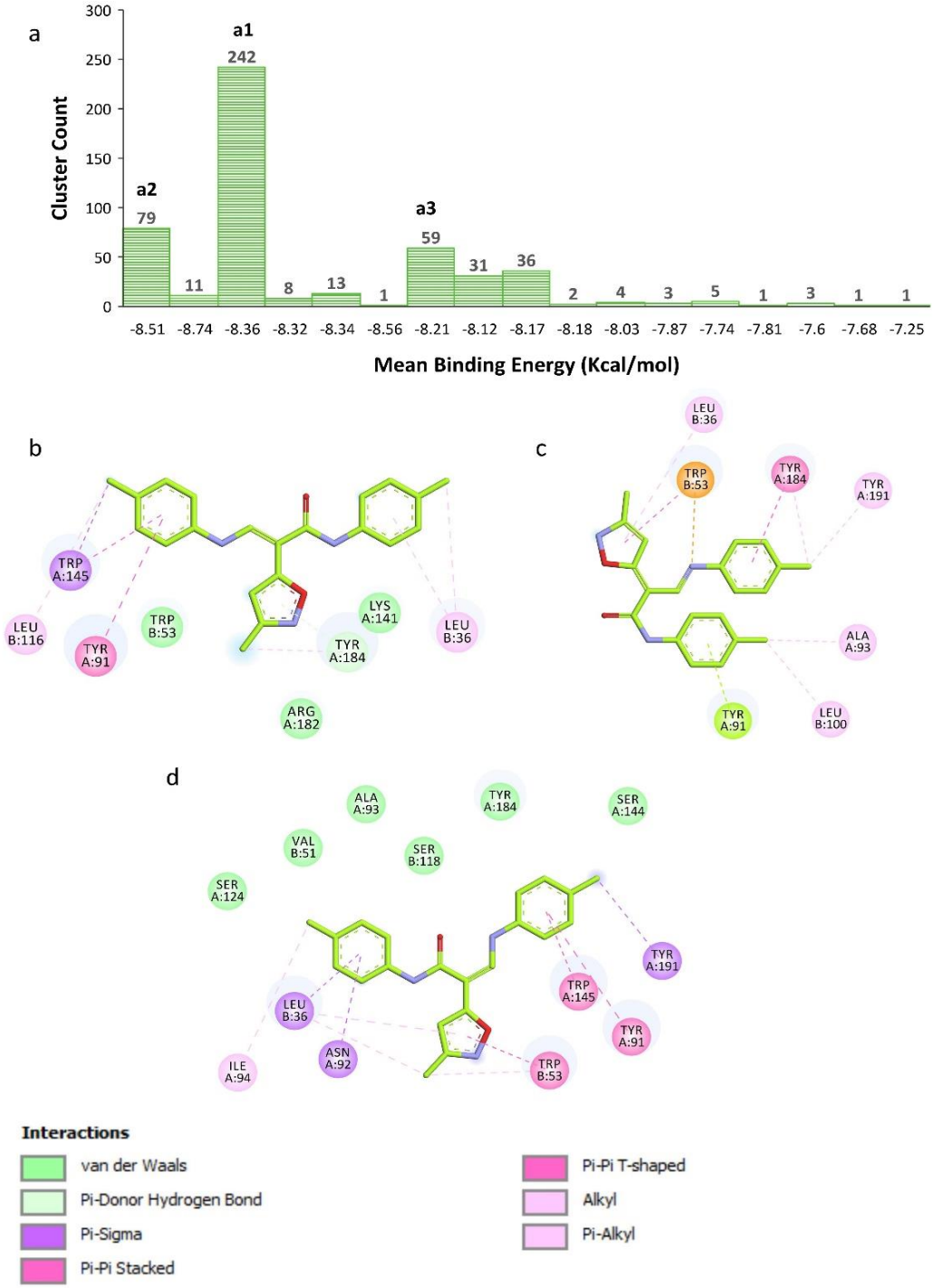

Figure 7.4 (a) Cluster distribution vs. mean binding energy of various poses of AVL-3288 in agonist sub-pocket of α7-nAChR (PDB id – 5AFK), (b, c, d, & e) 2-D interaction diagram of a1, a2, and a3 poses in agonist sub-pocket.

7.3.4. Alanine scanning

The results of alanine scanning are summarised in the figure (**Figure 7.5**). In case of top pocket, the t1 mode was subjected to alanine scanning by mutating ten critical interacting residues. The residues B:Arg4, A:Leu10 and A:Trp65 significantly contributed in binding

with loss of free energy of -2.699, -0.929, and -0.907 Kcal/mol, respectively. The other critical contributing residues were A:Leu6, A:Tyr14, A:Tyr62, and A:Leu63.

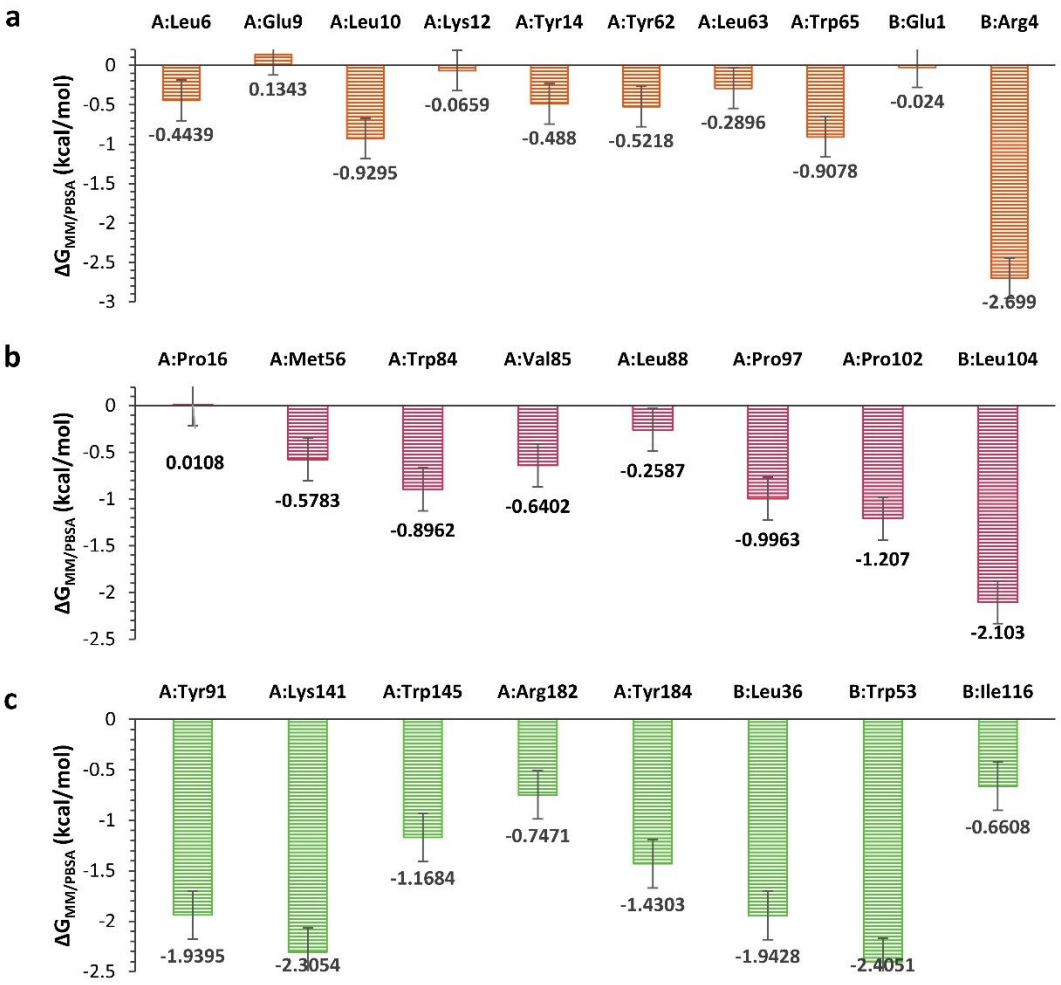

Figure 7.5 Virtual alanine scanning of (a) t1, (b) v1 and (c) a1 poses.

The v1 mode of binding in vestibule pocket of receptor displayed higher contribution of -2.103, -1.207 and -0.996 Kcal/mol due to B:Leu104, A:Pro102 and A:Pro97, respectively. These three residues, however, displayed π-alkyl and alkyl interactions. The other contributing residues were A:Met56, A:Trp84, A:Val85, and A:Leu88. The a1 binding mode of AVL-3288 in the sub-pocket near the agonist binding site displayed a stronger binding which were in line with the results of docking as well as MM/PBSA. The residues A:Tyr91, A:Lys141, B:Leu36 and B:Trp53 displayed binding energy of -1.939, -2.305, -1.942 and -2.405 Kcal/mol, respectively. The other residues including A:Trp145, A:Arg182, A:Try184 and B:Ile116 also displayed significant contribution in

binding. The three studies clearly indicated that AVL-3288 has higher affinity and stronger binding towards agonist sub-pocket and thus is responsible for the activation effect on α7-nAChR (**Figure 7.5**).

7.3.5. Molecular dynamics

MD simulation of the three selected binding modes was carried out to evaluate the efficiency of their binding, as well as to determine the actual site of action of AVL-3288 with α7-nAChR. The prepared systems were subjected to energy minimisation. The change in energy states of protein-ligand complexes of t1, v1 and a1 was found to be -173900, -173450 and -173980 to -271880, -272170 and -272130 Kcal/mol, respectively, which indicated that the energy minimisation protocol has substantially minimised the complexes. The heating of MD systems to a temperature of 310.15 K was attained at 28, 23 and 34 ps and density of the system attained to 1 g/cm^3 at 48, 52 and 51 ps, respectively for protein-ligand complexes of t1, v1 and a1, respectively. A short MD simulation run of 200 ps was used to check the stability and accuracy of the MD run. The simulations attained a stable RMSD at 100, 118 and 102 ps. The RMSD values for 50 ns simulation displayed that the stability of α7-nAChR-a1 complex was more stable than other complexes, especially after 30 ns of the simulation run. The RMSD plot for the α7-nAChR-v1 complex was stable but lesser than a1 pose. Further, α7-nAChR-t1 complex displayed fluctuating unstable trajectory compared to unbound α7-nAChR (**Figure 7.6(a)**). The RMSD of ligand at the three sites displayed a much clear picture. The a1 pose initially displayed a varying RMSD which was stabilised after 20 ns and remained stable till the end of the simulation run. While in the case of t1 and v1 poses, the RMSD remained less stable over the complete simulation run, which was higher in case of the top pocket. This clearly indicated that the binding of AVL-3288 was stabilised in sub-pocket near agonist binding site, thus may have the potential to act as a positive allosteric modulator of α7-nAChR (**Figure 7.6(b)**).

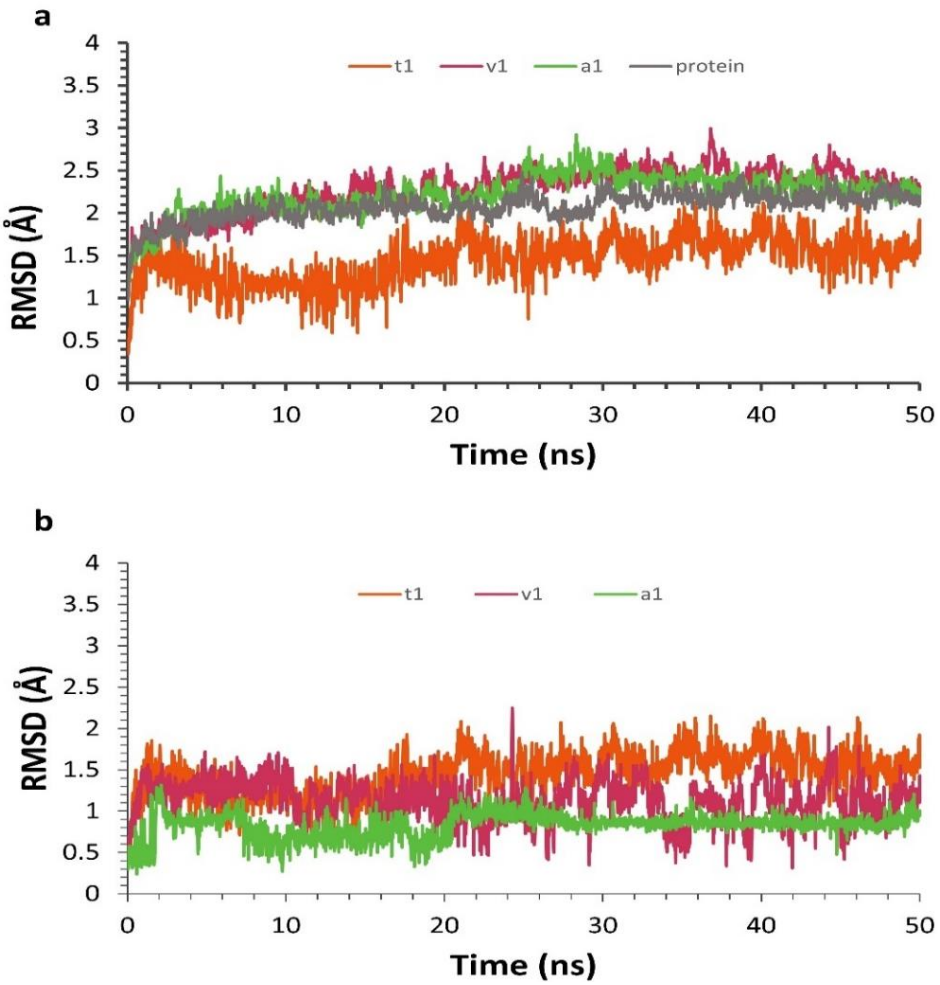

Figure 7.6 (a) RMSD deviation of Cα of protein backbone bound to poses of α7-nAChR AVL-3288 complex (t1, v1, a1) and unbound protein, (b) RMSD deviation of heavy atoms of t1, v1, a1 poses of AVL-3288 bound to α7-nAChR.

The results of Rg analysis indicated that all three complexes as well as free α7-nAChR had similar Rg during the simulation run. Therefore, it can be concluded that there is adequate stability in all the complexes, and no significant conformational change is observed in the protein backbone (**Figure 7.7(a)**). The average SASA(s) for complete MD simulation was found to be 20194.96, 20515.81, 20184.16 and 20358.89 $Å^2$ for t1, v1 and a1 complexes with α7-nAChR and α7-nAChR, respectively. The binding with t1 and a1 displayed a slight reduction in mean SASA compared to free α7-nAChR. This observation indicated that the binding was contributed by non-polar residues during the entire simulation run time for both modes. In the case of v1 mode, there was an increase

in mean SASA and was contrary to docking results, which displayed more contributions from non-polar residues toward receptor binding (**Figure 7.7(b)**).

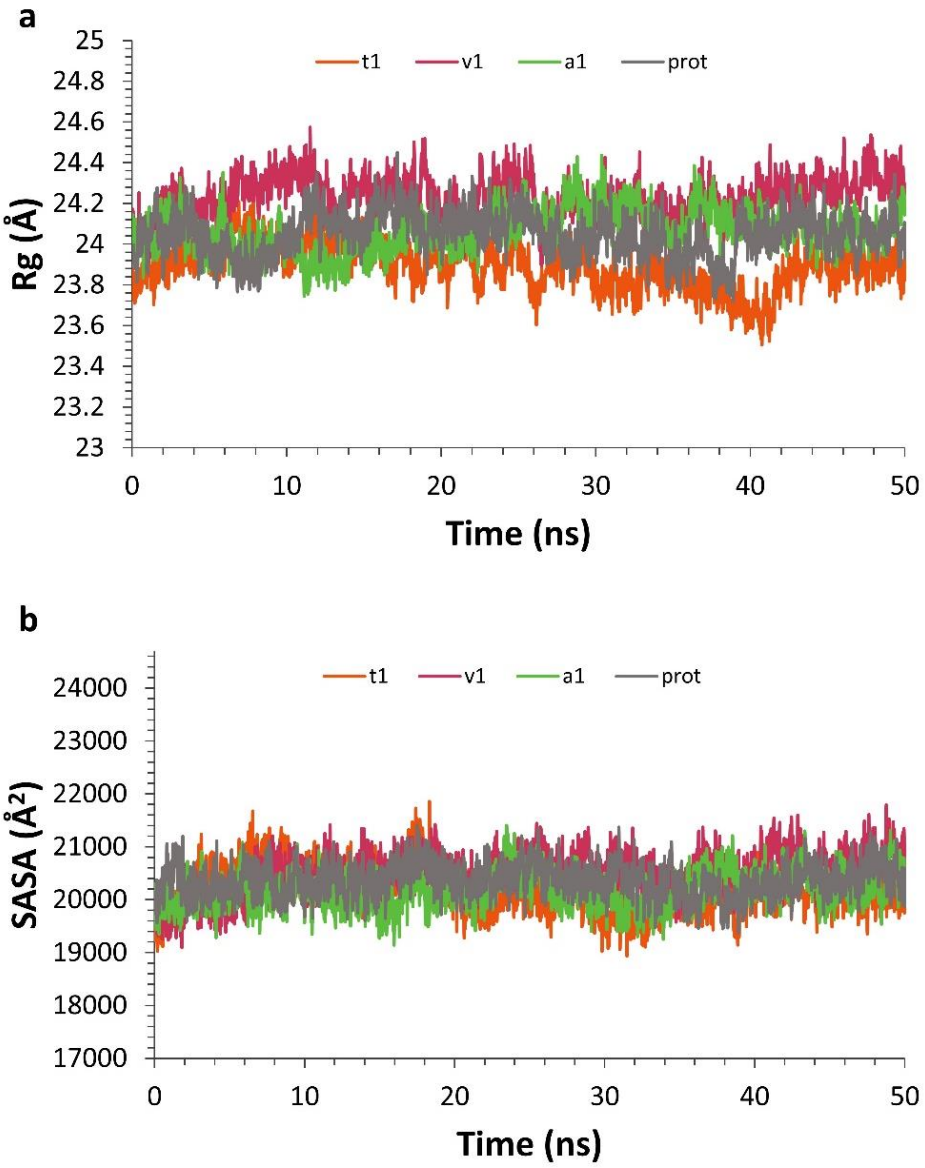

Figure 7.7 (a) Radius of gyration (Rg) of α7-nAChR AVL-3288 complex (t1, v1, a1) and unbound protein, (b) Solvent accessible surface area (SASA) of α7-nAChR AVL-3288 complex (t1, v1, a1) and unbound protein.

The protein-ligand binding is a thermodynamic phenomenon involving enthalpy changes due to various non-bonding interactions. These interactions contribute towards the strength of ligand binding. The t1 pose in the top pocket was found to have highest hydrogen bonding contribution with three primary residues i.e. A:Tyr71, A:Gln65 and A:Asn67 for a contact time of 49.04, 17.56 and 3.52%, respectively, of the total

simulation run. Further, the pose v1 displayed a minor contribution towards binding due to hydrogen bonding during the simulation run. Residues A:Tyr8 and B:Gln103 displayed hydrogen bonding for only 5.76 and 2.64% of simulation time, respectively. The most stable pose, a1, displayed hydrogen bonding with A:Arg138 and A:Arg185 for only 1.2 and 1.12% of the time, respectively, indicating that the v1 and a1 poses were stabilised due to non-covalent bond interaction other than hydrogen bonding (**Figure 7.8**).

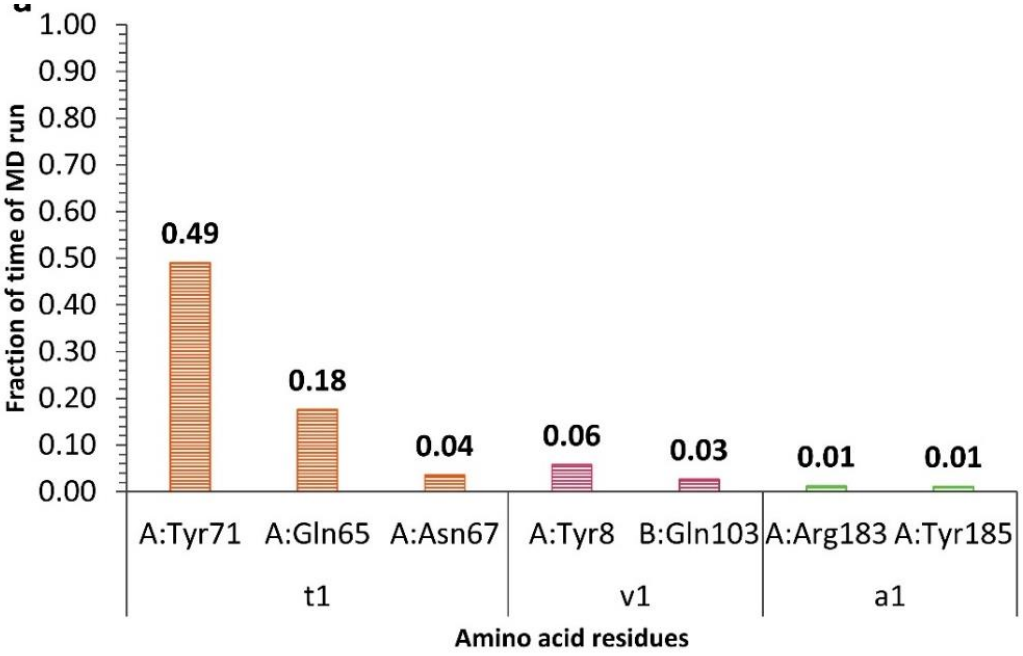

Figure 7.8 Fraction of time AVL3288 (t1, v1, a1) displayed hydrogen bonding with α7-nAChR amino acid residues.

7.3.6. MM-PBSA

The order of precedence for free energy calculations was found to be a1, t1, v1 for MM/PBSA. The mean $\Delta G_{MM/PBSA}$ energy was found to be better for a1 and t1 (**Table 7.1**). The results were quite different from docking studies, which may be due to the different solvation terms used in the two calculations.

The sub-pocket, besides the orthostatic binding pocket, is made up of β1, β2, β6 and loops between β8-β9 of the complementary subunit and only β4-β5 loop of the principal subunit. The docking results have a better binding with this site as well as in MM/PBSA. The MD study reflected stable RMSD for both proteins as well as **a1** pose of AVL-3288.

Further, no significant hydrogen bonding was observed during complete MD simulation, indicating the importance of π-interactions and van der Waals forces in binding.